A Letters Journal Exploring the Frontiers of Physics

April 2007

EPL, **78** (2007) 16003 www.epljournal.org
doi: 10.1209/0295-5075/78/16003

Interface reorientation during coherent phase transformations

V. I. Levitas[1], I. B. Ozsoy[1] and D. L. Preston[2]

[1] *Texas Tech University, Mechanical Engineering Department - Lubbock, TX 79409, USA*
[2] *Physics Division, Los Alamos National Laboratory - Los Alamos, NM 87545, USA*

received 7 December 2006; accepted in final form 21 February 2007
published online 19 March 2007

PACS 64.60.-i – General studies of phase transitions

Abstract – The universal thermodynamic driving force for coherent plane interface reorientation (IR) during first-order phase transformations (PT) in solids is derived. The relation between the rates of IR and interface propagation (IP) and the corresponding driving forces are derived for combined athermal and drag interface friction. The coupled evolution of IR and IP during cubic-tetragonal and tetragonal-orthorhombic PTs under three-dimensional loading is studied. An instability in the interface orientation is shown to have the features of a first-order PT.

Introduction. – The microstructure that is formed, *e.g.*, in ceramics, steels, or a shape memory alloy as a result of a solid-solid PT determines the physical and deformation properties of the material, internal stresses, and possible engineering applications. One of the goals of computational material design is the formation of a desired microstructure [1]. The universal (independent of specific constitutive relations) thermodynamic driving force for IP during solid-solid PT, the celebrated Eshelby driving force [2], and its generalization in the form of the tensor of chemical potential [3] have been known for decades. In marked contrast, the universal driving force for IR has not been previously obtained. The orientation of an invariant plane interface has initially been determined on the basis on crystallographic theory [4] which coincides with the results of direct energy minimization [5]. Orientation of an interface for linear elastic solids when it does not coincide with an invariant plane, *i.e.* when internal stresses are generated, and changes in its orientation under external stresses are studied in [6–10] using energy minimization. However, these methods explore specific expressions for elastic energy of the mixture of two phases when they are relatively simple. They cannot be used for important cases where athermal interface friction is significant. In this letter, an explicit universal (independent of specific constitutive relations) expression for the driving force for IR is derived for small and large strains. We derive an expression for the dissipation rate for simultaneous IP and IR that accounts for both athermal and drag interface friction. Relationships between the rates of IR and IP and the driving forces for IR and IP are obtained. Athermal friction introduces a nontrivial coupling between IR and IP. In particular, during IP, even an infinitesimal driving force for IR causes a finite IR rate. The nontrivial evolution of IR and IP during cubic-tetragonal and tetragonal-orthorhombic PTs under complex three-dimensional loading is studied numerically. An IR instability is revealed, *i.e.*, one interface orientation suddenly transforms to a significantly different one under complex loading. This rapid interface reorientation exhibits the features of a first-order PT, and is usually accompanied by a jump in the stresses and volume fractions. On the other hand, the IR is continuous under other types of loading. A change in temperature can induce IR as well.

Universal thermodynamic driving force for interface motion. – Consider a cube V containing two phases, 1 and 2, divided by a plane interface Σ with the unit normal $\boldsymbol{n}$ under external stresses. Let $\boldsymbol{\varepsilon}_i$ and $\boldsymbol{\sigma}_i$ be the constant strain and stress tensors in each phase, then

$$\boldsymbol{\varepsilon} = c_i\boldsymbol{\varepsilon}_i, \qquad \boldsymbol{\sigma} = c_i\boldsymbol{\sigma}_i, \qquad \psi = c_i\psi_i(\boldsymbol{\varepsilon}_i,\theta), \qquad s = c_i s_i(\boldsymbol{\varepsilon}_i,\theta) \tag{1}$$

are the strain and stress tensors, as well as the Helmholtz free energy and entropy, both per unit volume, averaged over V, c_i is the volume fraction of the i-th phase, θ is the temperature homogeneous in V, and summation over the repeated subscript is assumed. As is usual for strain-dominated PTs with coherent interfaces (displacements are continuous across an interface), we neglect the interface energy (and its orientational dependence) in comparison to the elastic energy. It follows from the thermodynamics of each phase that $\boldsymbol{\sigma}_i = \partial\psi_i/\partial\boldsymbol{\varepsilon}_i$ and $s_i = -\partial\psi_i/\partial\theta$. The dissipation rate per unit volume is $D_V = \boldsymbol{\sigma} : \dot{\boldsymbol{\varepsilon}} - \dot{\psi} - s\dot{\theta} \geqslant 0$, where **:** designates double contraction of tensors. Inserting in D_V the expressions

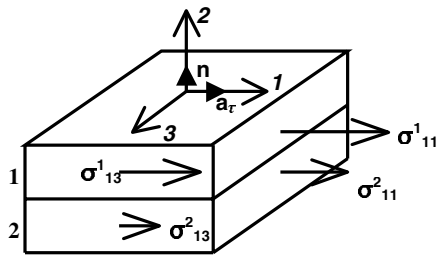

Fig. 1: Components of the stress tensor that are discontinuous across the interface Σ and therefore contribute to $\boldsymbol{X}_n$, the driving force for IR.

for $\boldsymbol{\varepsilon}$ and ψ from (1), we obtain

$$D_V = X_c\dot{c}_2 + c_i(\boldsymbol{\sigma}-\boldsymbol{\sigma}_i):\dot{\boldsymbol{\varepsilon}}_i \geqslant 0, \tag{2}$$

where $X_c := \boldsymbol{\sigma}:[\boldsymbol{\varepsilon}] - [\psi]$ is the Eshelby driving force for IP during the PT $1 \leftrightarrow 2$ and $[\boldsymbol{A}] := \boldsymbol{A}_2 - \boldsymbol{A}_1$. Using $\boldsymbol{\sigma} = c_i\boldsymbol{\sigma}_i$, and the traction continuity and Hadamard compatibility conditions

$$[\boldsymbol{\sigma}]\cdot\boldsymbol{n} = 0, \qquad [\boldsymbol{\varepsilon}] = (\boldsymbol{a}\boldsymbol{n})_s, \tag{3}$$

where the vector $\boldsymbol{a}$ characterizes the strain jump and the subscript s means symmetrization, the second term in (2) can be transformed into $\boldsymbol{X}_n\cdot\dot{\boldsymbol{n}}$, where

$$\boldsymbol{X}_n := -c_1c_2\boldsymbol{a}\cdot[\boldsymbol{\sigma}] \tag{4}$$

is the expression for the universal thermodynamic driving force for IR. Thus,

$$D_V = X_c\dot{c}_2 + \boldsymbol{X}_n\cdot\dot{\boldsymbol{n}} \geqslant 0. \tag{5}$$

Decomposing $\boldsymbol{a} = \boldsymbol{a}_n + \boldsymbol{a}_\tau$, where $\boldsymbol{a}_n$ and $\boldsymbol{a}_\tau$ are collinear and orthogonal to $\boldsymbol{n}$ (fig. 1), and using $\boldsymbol{n}\cdot[\boldsymbol{\sigma}] = 0$, we obtain

$$\boldsymbol{X}_n = -c_1c_2\boldsymbol{a}_\tau\cdot[\boldsymbol{\sigma}]. \tag{6}$$

Thus, the normal component of the strain discontinuity across the interface does not induce IR; only the shear (volume-preserving) component contributes to $\boldsymbol{X}_n$. Also, $\boldsymbol{X}_n\cdot\boldsymbol{n} = 0$ because of $[\boldsymbol{\sigma}]\cdot\boldsymbol{n} = 0$, *i.e.*, $\boldsymbol{X}_n$ lies in the interface. In the coordinate system where $\boldsymbol{a}_\tau = |\boldsymbol{a}_\tau|(1,0,0)$ and $\boldsymbol{n} = (0,1,0)$ (fig. 1) we have

$$X^1_n = -c_1c_2|\boldsymbol{a}_\tau|[\sigma_{11}] \qquad \text{and} \qquad X^3_n = -c_1c_2|\boldsymbol{a}_\tau|[\sigma_{13}], \tag{7}$$

i.e., the discontinuities in only two components of $\boldsymbol{\sigma}$ contribute to $\boldsymbol{X}_n$. Thus, the conditions for thermodynamic orientational equilibrium are $[\sigma_{11}] = [\sigma_{13}] = 0$ or $\boldsymbol{a}_\tau = 0$. Following a similar approach for the case of large strain, we obtain

$$\boldsymbol{X}_n := -c_1c_2\boldsymbol{a}\cdot[\boldsymbol{P}], \tag{8}$$

where $\boldsymbol{P}$ is the nonsymmetric Piola-Kirchoff (nominal) stress tensor (*i.e.* the force per unit area in the undeformed state), and $\boldsymbol{a}$ is determined by the equation for the jump in the deformation gradient $[\boldsymbol{F}] = \boldsymbol{a}\boldsymbol{n}$. Since $\boldsymbol{P}$ is not symmetric, $[\boldsymbol{P}]\cdot\boldsymbol{n} = 0$ but $\boldsymbol{n}\cdot[\boldsymbol{P}] \neq 0$, it is not valid to substitute $\boldsymbol{a}_\tau$ for $\boldsymbol{a}$.

For each phase we assume Hooke's law, $\boldsymbol{\sigma}_i = \boldsymbol{E}_i:\varepsilon^e_i$, where $\boldsymbol{E}_i$ is the fourth-rank elasticity tensor, and $\boldsymbol{\varepsilon}^e_i := \boldsymbol{\varepsilon}_i - \boldsymbol{\varepsilon}^t_i$ and $\boldsymbol{\varepsilon}^t_i$ are the elastic and transformation (eigen) strains; $\boldsymbol{\varepsilon}^t_1 = 0$ by definition, hence $\boldsymbol{\varepsilon}^t := \boldsymbol{\varepsilon}^t_2$. Transformation strain transforms crystal lattice of the parent phase into lattice of the product phase; if phase 1 is considered as a parent phase, then $\boldsymbol{\varepsilon}^t_1 = 0$. When $\boldsymbol{E}_1 = \boldsymbol{E}_2 = \boldsymbol{E}$ and $\boldsymbol{\varepsilon}^t_i$ are independent of the applied stress $\boldsymbol{\sigma}$, then $\boldsymbol{\sigma}_i = \boldsymbol{\sigma} + \boldsymbol{\sigma}^{in}_i$, where $\boldsymbol{\sigma}^{in}_i$ are the internal stresses due to $\boldsymbol{\varepsilon}^t_i$ ($c_i\boldsymbol{\sigma}_i = 0$) that are independent of $\boldsymbol{\sigma}$ [11]. Then $[\boldsymbol{\sigma}] = [\boldsymbol{\sigma}^{in}]$, thus $\boldsymbol{X}_n$ is independent of $\boldsymbol{\sigma}$ as well. If the interface is an invariant plane for $\boldsymbol{\varepsilon}^t$ [5], *e.g.*, between two twins, then $\boldsymbol{\sigma}^{in} = 0$ and again the external stresses will not cause IR. Thus, for equal linear elastic properties of phases and stress-independent transformation strain, external stresses do not effect IR. This is generally not true for equal nonlinear elastic properties (because the principle of linear superposition cannot be applied), unequal elastic properties, and when $\boldsymbol{\varepsilon}^t_i$ depends on $\boldsymbol{\sigma}$ (*e.g.* when one phase consists of a fine-scale mixture of several crystallographically equivalent variants [10] or when plastic accommodation occurs).

Dissipation rate. – The dissipation rate at each point of the moving interface is assumed to be the sum of athermal, $\mathcal{D}_a$, and viscous, $\mathcal{D}_v$, friction components: $\mathcal{D} = \mathcal{D}_a + \mathcal{D}_v = k|v_n| + \lambda v_n^2$. Here v_n is the normal interface velocity, k is the athermal interface friction due to interaction between the interface and the long-range stress fields of defects (point defects, dislocations, grain and subgrain boundaries), as well as the Peierls barrier, and λ is the viscosity coefficient. Other contributions, for example, dissipation due to thermally activated motion of the interface past obstacles, can be similarly taken into account. The dissipation rate per unit volume due to the motion of the interface is $D = \int_\Sigma \mathcal{D}\mathrm{d}\Sigma/V = D_a + D_v$. For a plane interface, the normal velocity at the point $\boldsymbol{r}$ can be expressed as $v_n = v_{0n} + \boldsymbol{\omega}\times(\boldsymbol{r}-\boldsymbol{r}_0)\cdot\boldsymbol{n}$, where $\boldsymbol{r}_0$ is the centroid of the interface in V, $v_{0n} = \dot{\boldsymbol{r}}_0\cdot\boldsymbol{n}$ is the normal velocity of the centroid, and $\boldsymbol{\omega} = \boldsymbol{n}\times\dot{\boldsymbol{n}}$ ($|\boldsymbol{\omega}| = |\dot{\boldsymbol{n}}|$) is the angular velocity of the interface. To obtain all results analytically, we consider IR in the plane 1-2. In this case, $v_n = v_{0n} + \omega r$, where r is the distance from the interface centroid in the plane 1-2, $[\sigma_{13}] = 0$, $\boldsymbol{X}_n = X_n\boldsymbol{a}_\tau/|\boldsymbol{a}_\tau|$, and $\boldsymbol{X}_n\cdot\dot{\boldsymbol{n}} = X_n\omega$. When evaluating D_a, one needs to consider separately the cases when the position of the center of rotation $r_c = -v_{0n}/\omega$ belongs to the interface ($-R \leqslant r_c \leqslant R$, where $2R$ is the interface length in the plane 1-2), or does not, *i.e.* when v_n is of fixed sign or changes sign within the interface. Substituting v_n in the expression for D and defining $\omega_0 = v_{0n}/R$ we obtain

$$\begin{aligned} D_a &= A|\omega|(1+\omega_0^2/\omega^2) \quad \text{for } |\omega_0/\omega| \leqslant 1, \\ D_a &= 2A|\omega_0| \quad \text{for } |\omega_0/\omega| > 1; \\ D_v &= B\omega^2(1+3\,\omega_0^2/\omega^2), \end{aligned} \tag{9}$$

where $A = kR^2/S$, $B = 2\lambda R^3/(3S)$, and S is the area of the cube face. On the other hand, since $\dot{c}_2 = v_{0n}\Sigma/V$, then using eq. (5) we obtain $\tilde{D} := D/A = D_V/A = (X_c v_{0n}\Sigma/V + X_n\omega)/A = \tilde{X}_c\omega_0 + \tilde{X}_n\omega$, where $\tilde{X}_c = X_c \times R\Sigma/(AV)$ and $\tilde{X}_n = X_n/A$. Decomposing the $\tilde{X}$ into athermal and viscous parts, $\tilde{X}_c = \tilde{X}_c^a + \tilde{X}_c^v$ and $\tilde{X}_n = \tilde{X}_n^a + \tilde{X}_n^v$, we obtain

$$\begin{aligned} \tilde{D}_a &:= D_a/A = \tilde{X}_c^a\omega_0 + \tilde{X}_n^a\omega = \tilde{\boldsymbol{X}}^a\cdot\bar{\boldsymbol{\omega}}, \\ \tilde{D}_v &:= D_v/A = \tilde{X}_c^v\omega_0 + \tilde{X}_n^v\omega = \tilde{\boldsymbol{X}}^v\cdot\bar{\boldsymbol{\omega}}, \end{aligned} \tag{10}$$

where D_a and D_v are given by eq. (9), $\bar{\boldsymbol{\omega}} := (\omega_0, \omega)$, $\tilde{\boldsymbol{X}}^a := (\tilde{X}_c^a, \tilde{X}_n^a)$, $\tilde{\boldsymbol{X}}^v := (\tilde{X}_c^v, \tilde{X}_n^v)$, and $\tilde{\boldsymbol{X}} = \tilde{\boldsymbol{X}}^a + \tilde{\boldsymbol{X}}^v$. The two eqs. (10) are not sufficient to find the four scalar driving forces $\tilde{\boldsymbol{X}}^a$, $\tilde{\boldsymbol{X}}^v$. Applying the extremum principles of nonlinear irreversible thermodynamics [12] (which can be justified using the postulate of realizability [13]), we obtain

$$\tilde{X}_c^a = \frac{\partial\tilde{D}_a}{\partial\omega_0} = \begin{cases} 2\omega_0/\omega\,\mathrm{sign}(\omega) & \text{for } |\omega_0/\omega| \leqslant 1, \\ 2\,\mathrm{sign}(\omega_0) & \text{for } |\omega_0/\omega| > 1, \end{cases}$$

$$\tilde{X}_n^a = \frac{\partial\tilde{D}_a}{\partial\omega} = \begin{cases} (1-\omega_0^2/\omega^2)\,\mathrm{sign}(\omega) & \text{for } |\omega_0/\omega| \leqslant 1, \\ 0 \quad \text{for } |\omega_0/\omega| > 1, \end{cases} \tag{11}$$

$$\begin{aligned} \tilde{X}_c^v &= (1/2)\,\partial\tilde{D}_v/\partial\omega_0 = 3C\omega_0, \\ \tilde{X}_n^v &= (1/2)\,\partial\tilde{D}_v/\partial\omega = C\omega, \quad C := B/A. \end{aligned} \tag{12}$$

The important point here is to assume thermodynamic independence of athermal and viscous dissipation, otherwise no reasonable result can be obtained. Let us consider the case $\tilde{\boldsymbol{X}}^v \ll \tilde{\boldsymbol{X}}^a$, which corresponds to neglect of viscosity ($C = 0$) or slow interface motion (IM = IP + IR). Eliminating ω_0/ω from eq. (11) for $|\omega_0/\omega| \leqslant 1$, one obtains the equations of the limit curve for IM in the $\tilde{X}_n^a$-$\tilde{X}_c^a$ plane (fig. 2)

$$f_\pm(\tilde{\boldsymbol{X}}^a) := \tilde{X}_n^a \mp [1 - (1/4)\,(\tilde{X}_c^a)^2] = 0. \tag{13}$$

The case $|\omega_0/\omega| > 1$ yields just $\tilde{\boldsymbol{X}}^a = (\pm 2, 0)$. Inside the curve (13), *i.e.*, for $f < 0$, where $\omega_0 = \omega = 0$, IM does not occur. The curve $f = 0$ is the counterpart of the stress-space yield surface in single and polycrystalline plasticity or the friction surface [12,13], or the PT surface [11]. We have $\boldsymbol{\nabla} f_\pm = (\pm\tilde{X}_c^a/2, 1) = (\omega_0/\omega, 1) \sim (\omega_0, \omega)$, *i.e.*,

$$\bar{\boldsymbol{\omega}} = h\,\boldsymbol{\nabla} f \tag{14}$$

with h a constant and $\boldsymbol{\nabla}$ for gradient operator. Expression (14) is the associated PT rule, similar to one in plasticity, friction and PT theory [11–13]. Thus, the vector $\bar{\boldsymbol{\omega}}$ is a normal to the limit curve $f = 0$ (fig. 2). At the singular points $\tilde{\boldsymbol{X}}^a = (\pm 2, 0)$ the vector $\bar{\boldsymbol{\omega}}$ must lie on or between the normals to f_+ and f_-, which are inclined $\pm 45°$ to the $\tilde{X}_c^a$ axis (fig. 2). Since $|\dot{\boldsymbol{n}}| = \omega$ must vanish for $\tilde{X}_n^a = 0$, $\bar{\boldsymbol{\omega}}$ is in fact along the $\tilde{X}_c^a$-axis. However, for any infinitesimal $\tilde{X}_n^a$ we get $\omega_0/\omega = 1$, *i.e.* ω jumps to a finite value. This

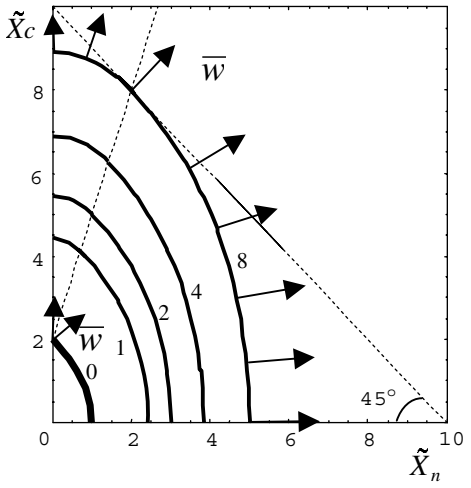

Fig. 2: Plots of the potential contours $\Psi(\tilde{\boldsymbol{X}}) = M$ for the values of M shown near the curves. The contours are symmetric with respect to the $\tilde{X}_n$ and $\tilde{X}_c$ axes. The contour $\Psi = 0$ coincides with $f = 0$ (eq. (13)), inside of which IM does not occur. The velocity vector $\bar{\boldsymbol{\omega}}$ is orthogonal to the potential contours; its magnitude is proportional to the inverse distance between nearest curves along $\bar{\boldsymbol{\omega}}$. The straight line $\tilde{X}_c - 3\tilde{X}_n = 2$ corresponds to the condition $\omega_0 = \omega$. The curves above the line $\tilde{X}_c - 3\tilde{X}_n = 2$ are ellipses.

means that during the IP, the IR occurs fast until the thermodynamic equilibrium orientation determined by $\tilde{X}_n^a = 0$ is reached. Also, in the case $\tilde{\boldsymbol{X}}^a \ll \tilde{\boldsymbol{X}}^v$, *i.e.*, small athermal friction or large viscosity, eq. (12) shows that there is no coupling between IP and IR. Note, for any $\tilde{X}_n^a \neq 0$, the center of interface rotation belongs to the interface and $|\omega_0/\omega| \leqslant 1$.

Consider now a system in thermodynamic equilibrium with $\tilde{X}_n^a \neq 0$ and $f < 0$, and increase $|\tilde{X}_c^a|$ by changing the temperature until $f = 0$. Then, IR will occur along with IP until $\tilde{X}_n^a = 0$. Since $|\tilde{X}_c^a| = 2\sqrt{1 - |\tilde{X}_n^a|}$, a rotational driving force ($\tilde{X}_n^a \neq 0$) can significantly reduce the magnitude of the driving force required for IP.

With viscous friction, eqs. (11)-(12) are of the form $\tilde{\boldsymbol{X}}(\bar{\boldsymbol{\omega}}) = \mathrm{d}\Phi/\mathrm{d}\bar{\boldsymbol{\omega}}$, where $\Phi = \tilde{D}_a + \tilde{D}_v/2$. Using the Lagrange transformation $\Psi(\tilde{\boldsymbol{X}}) = \tilde{\boldsymbol{X}}\cdot\bar{\boldsymbol{\omega}}(\tilde{\boldsymbol{X}}) - \Phi(\bar{\boldsymbol{\omega}}(\tilde{\boldsymbol{X}}))$, one can invert the relations between $\bar{\boldsymbol{\omega}}$ and $\tilde{\boldsymbol{X}}$: $\bar{\boldsymbol{\omega}} = \mathrm{d}\Psi/\mathrm{d}\tilde{\boldsymbol{X}}$, where

$$\begin{aligned} \Psi(\tilde{\boldsymbol{X}}) \;=\; & g_3[2^{2/3}g_4(\tilde{X}_n - (1 + 1/(18\,2^{1/3}g_4^2)) \\ & -2^{1/3}g_3g_4^2(1 + 1/(6\,2^{1/3}g_4^2)) + \tilde{X}_c/3]/C \\ & \text{for } \tilde{X}_c - 3\tilde{X}_n \leqslant 2; \\ \Psi(\tilde{\boldsymbol{X}}) \;=\; & ((\tilde{X}_c - 2)^2 + 3\tilde{X}_n^2)/(6C) \\ & \text{for } \tilde{X}_c - 3\tilde{X}_n > 2. \end{aligned} \tag{15}$$

Here $g_1 = (9\tilde{X}_c + (81\tilde{X}_c^2 + 4(3\tilde{X}_n - 1)^3)^{1/2})^{1/3}$, $g_2 = 2 - 6\tilde{X}_n + 2^{1/3}g_1^2$, $g_3 = \tilde{X}_c - 2^{1/3}/(3g_4)$, and $g_4 = g_1/g_2$. For $\tilde{X}_c$, $\tilde{X}_n > 0$, (first quadrant in the PT space) $\bar{\boldsymbol{\omega}}(\tilde{\boldsymbol{X}})$

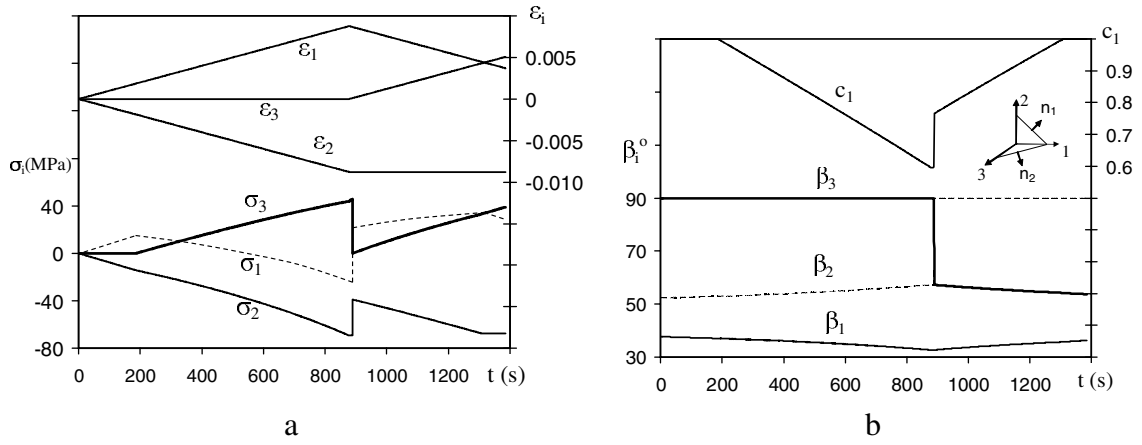

Fig. 3: (a) Prescribed strain history and the corresponding stresses, and (b) the evolution of the volume fraction c_1 and the direction angles, β_i, between $\boldsymbol{n}$ and the coordinate axes for a tetragonal-orthorhombic PT. The jump in the normal is accompanied by a jump in volume fraction (reverse PT) and all macroscopic stresses.

is given by

$$\begin{aligned}&\omega_0 = g_3/(3C), \quad \omega = 2^{2/3} g_3\, g_4/C \quad \text{for } \tilde{X}_c - 3\tilde{X}_n \leqslant 2;\\ &\omega_0 = (\tilde{X}_c - 2)/(3C), \quad \omega = \tilde{X}_n/C \quad \text{for } \tilde{X}_c - 3\tilde{X}_n > 2;\end{aligned} \tag{16}$$

they are symmetric with respect to the coordinate axes. A geometric representation of eqs. (15)-(16) is given in fig. 2. Viscosity regularizes the singular point on the limit curve $f = 0$ (or $\Psi = 0$) and removes the jump in the $\bar{\boldsymbol{\omega}}$ vector. Outside the limit curve $f = 0$, an infinitesimal $\tilde{X}_n$ causes an infinitesimal IR rate.

Coupled evolution of IP **and** IR**: orientational instability.** – The complete system of equations describing the evolution of stresses and strains in each phase, IP (or volume fraction), and IR for a prescribed macroscopic strain (or stress) - temperature path consists of eqs. (1), (3), (4), the Eshelby driving force, Hooke's law, the free energies $\psi_i = (1/2)\boldsymbol{\varepsilon}_i^e : \boldsymbol{E}_i : \boldsymbol{\varepsilon}_i^e + \psi_i^\theta$ ($\psi_i^\theta(\theta)$ is the thermal part of the free energy), and the kinetic eqs. (16). The stresses and strains in the phases can be found analytically [11]. Phase and orientational equilibrium configurations can be determined from the conditions $X_c = X_n = 0$; assuming phases with equal isotropic elastic moduli and $k = 0$, we obtained analytic solutions for cubic-tetragonal and tetragonal-orthorhombic PTs that coincide with those presented in [6]. We have also obtained analytical solutions for cubic-orthorhombic PTs, but they are too complex to be presented here.

Two classes of numerical simulations were carried out to illustrate the phenomenology of IR: two calculations of IR during tetragonal-orthorhombic PTs with $\boldsymbol{\varepsilon}^t = \{0.022; -0.011;\ -0.0044\}$ and $k = 0$ for quasi-static loading; and two calculations for cubic-tetragonal PTs with $\boldsymbol{\varepsilon}^t = \{0.022; -0.011; -0.011\}$ and $k > 0$ for $\dot{\varepsilon}_1 = 0.0025\,\mathrm{s}^{-1}$. The following material properties were used in all seven calculations: Young's moduli, $E_1 = 10\,\mathrm{GPa}$ and $E_2 = 40\,\mathrm{GPa}$; Poisson's ratio, $\nu_1 = \nu_2 = 0.3$; and the

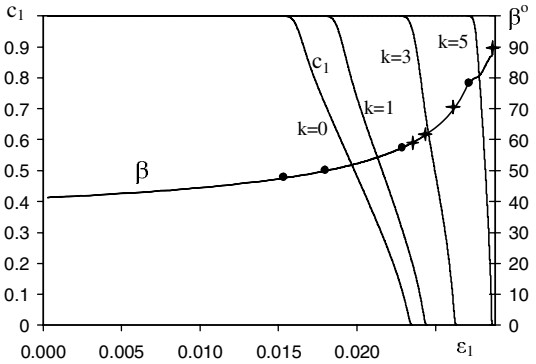

Fig. 4: Variation of the volume fraction c_1 and the angle β between the normal and the cubic axis 1 for various k (shown near the curves) for a cubic-tetragonal PT and the loading path $\varepsilon_2 = \varepsilon_3 = -\nu\varepsilon_1$. Dots and crosses designate PT start and finish, respectively. For $k = 0$ and $k \neq 0$, β varies along the same curve in the nucleus (since it is determined from $\boldsymbol{X}_n = 0$). During the PT, curves with different k partially overlap, but they begin and end with larger β for larger k, since the PT starts and finishes at larger strains. For $k = 5\,\mathrm{MPa}$ the change in β from both the nucleus and the PT is 49°.

coefficient of viscosity $\lambda = 0.3\,\mathrm{MPa\,s/m}$. The interface length $2R$ was determined from the geometry for the unit cube.

For each simulation, a nucleus with $c_2 = 10^{-4}$ was introduced by locating the planar interface Σ very near a corner of the cube. The initial interface orientation, $\boldsymbol{n}_0$, was either determined from the condition $\boldsymbol{X}_n = 0$, which gives the "optimal" (energy minimizing) orientation, or assigned a non-optimal value. The justification for using a non-optimal $\boldsymbol{n}_0$ is as follows. Nucleation usually occurs at defects, *e.g.*, certain dislocation configurations, therefore the sum of the applied stress and the stress field of the defect must be used in the condition $\boldsymbol{X}_n = 0$. Thus, a non-optimal $\boldsymbol{n}_0$ mimics the presence of a defect stress field.

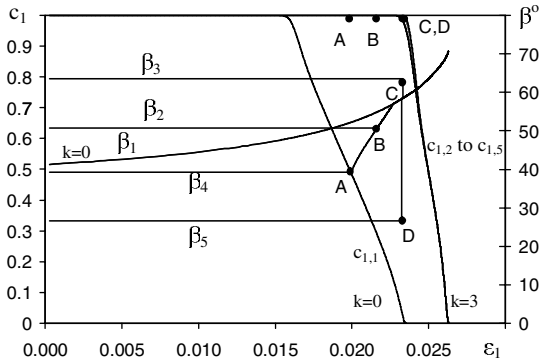

Fig. 5: Variations of the volume fraction c_1 and the normal orientation β for $k = 0, 3\,\mathrm{MPa}$ for the loading path $\varepsilon_2 = \varepsilon_3 = -\nu\varepsilon_1$ and cubic-tetragonal PT. The curves for β_1 (β_2–β_5) and c_1^1 (c_1^2–c_1^5) correspond to $k = 0$ ($k = 3$). The orientations β_1 and β_2–β_5 are for optimal and non-optimal $\boldsymbol{n}_0$ in the nucleus, respectively. The points A, B, C, and D designate the start of a PT. For $\beta_0 = 63^\circ$ and $\beta_0 = 27^\circ$, cases 3 and 5, the start of the PT is accompanied by an orientational instability and a jump from C or D to the optimal orientation, β_1. After the start of the PT for $\beta_0 = 39^\circ$ and $\beta_0 = 51^\circ$, cases 4 and 2, at A and B, there is a rapid increase in β but a very small change in c_1 until the normal reaches the optimal orientation ($\boldsymbol{X}_n = 0$). After this, β continues to rise while c_1 quickly decreases to zero. Note that for $k = 3\,\mathrm{MPa}$ the PT runs to completion along the same curve for all β_0.

When the nucleus grows away from the defect, the effect of the nucleating defect becomes negligible.

The tetragonal-orthorhombic PT was studied for prescribed strains corresponding to the uniaxial tensile stress σ_3 ($\sigma_1 = \sigma_2 = 0$), $c_1 = 0.7014$ was held constant (no IP) by changing the temperature, and $[\psi^\theta]$ was determined from $X_c = 0$. The initial equilibrium interface normal corresponding to $\boldsymbol{X}_n = 0$ was $\boldsymbol{n}_1 = (a, b, 0)$, where $a = 0.79$ and $b = 0.61$. Due to symmetry there are three crystallographically, but not energetically, equivalent normals $\boldsymbol{n}_i$ obtained by cyclic permutation of the components of $\boldsymbol{n}_1$. The Gibbs energy has a multiwell structure in the space of the $\boldsymbol{n}_j$: the local minima are located at $\boldsymbol{n}_i$ and are separated by potential barriers. For the tensile stress σ_3 the Gibbs energy is minimized for $\boldsymbol{n}_2 = (a, 0, b)$. However, during loading up to $\varepsilon_3 < 0.004$, the normal does not change because the local energy minimum at $\boldsymbol{n}_1$ is separated from the stable energy minimum at $\boldsymbol{n}_2$ by a finite potential barrier. At $\varepsilon_3 = 0.004$ the minimum at $\boldsymbol{n}_1$ and the potential barrier disappear, hence an abrupt IR occurs to the stable normal $\boldsymbol{n}_2$. Further loading does not induce additional IR. Thus, we find that an instability in the interface normal leads to a rapid interface reorientation that has the following features of a first-order PT: there are multiple energy minima that are separated by an energy barrier, and when the barrier disappears, the system abruptly evolves toward another stable state. Figures 3–5 show examples of PT under tri-axial staining. In fig. 3 a jump in orientation is accompanied by a jump in volume fraction and all macroscopic stresses, fig. 4 exhibits a large continuous variation in the normal orientation, and fig. 5 shows a PT with non-optimal $\boldsymbol{n}_0$ in the nucleus.

To summarize, the universal driving force for plane IR during a coherent PT was derived for small and large strains. Explicit relationship between the rate of IP and IR and the driving forces for IP and IR are obtained. We presented nontrivial examples of combined IP and IR that will hopefully motivate related experimental studies. A generalization that accounts for plastic accommodation by slip and twinning will be presented elsewhere. The equations obtained here are expected to provide a more accurate description of discrete microstructure formation than the equations in [11].

* * *

LANL, NSF (CMS-0555909) and TTU support for VIL and IBO are gratefully acknowledged.

REFERENCES

[1] Olson G. B., *Science*, **277** (1997) 1237.
[2] Eshelby J. D., *Inelastic Behaviour of Solids*, edited by Kanninen M. F. *et al.*, Vol. **77** (McGraw Hill, New York) 1970.
[3] Grinfeld M. A., *Thermodynamic Methods in the Theory of Heterogeneous Systems* (Longman, London) 1991.
[4] Wayman C. M., *Introduction to the Crystallography of Martensitic Transformation* (Macmillan, New York) 1964.
[5] Bhattacharya K., *Microstructure of Martensite* (Oxford University Press, New York) 2004.
[6] Roytburd A. L. and Kosenko N. S., *Phys. Status Solidi (A)*, **35** (1976) 735.
[7] Roytburd A. L. and Kosenko N. S., *Scr. Metall.*, **11** (1977) 1039.
[8] Roytburd A. L., *Sov. Phys. Crystallogr.*, **26** (1983) 628.
[9] Roytburd A. L. and Slutsker J., *Physica B*, **233** (1997) 390.
[10] Roytburd A. L. and Slutsker J., *J. Mech. Phys. Solids*, **49** (2001) 1795.
[11] Levitas V. I., Idesman A. V. and Preston D., *Phys. Rev. Lett.*, **93** (2004) 105701; Idesman A. V., Levitas V. I., Preston D. L. and Cho J.-Y., *J. Mech. Phys. Solids*, **53** (2005) 495.
[12] Ziegler H., *An Introduction to Thermomechanics* (North-Holland, Amsterdam) 1977.
[13] Levitas V. I., *Int. J. Eng. Sci.*, **33** (1995) 921.